Journal of Physiology (1989), **410**, *pp.* 227–249
With 12 text-figures
Printed in Great Britain

MEASUREMENT OF REVERSAL POTENTIAL OF Na^+–Ca^{2+} EXCHANGE CURRENT IN SINGLE GUINEA-PIG VENTRICULAR CELLS

BY TSUGUHISA EHARA, SATOSHI MATSUOKA* AND AKINORI NOMA

*From the Department of Physiology, Faculty of Medicine, Kyushu University, Fukuoka 812, Japan and *Department of Internal Medicine, Tottori University School of Medicine, Yonago 683, Japan*

(*Received 1 June 1988*)

SUMMARY

1. To identify the Na^+- or Ca^{2+}-induced current as Na^+–Ca^{2+} exchange current and to determine the stoichiometry of the Na^+–Ca^{2+} exchange, the reversal potential was measured in a wide range of external Na^+ ($[Na^+]_o$) or Ca^{2+} ($[Ca^{2+}]_o$) concentrations. The Na^+- or Ca^{2+}-induced current was recorded in single ventricular cells enzymatically dispersed from guinea-pig hearts, using the technique of whole-cell voltage clamp combined with internal perfusion.

2. In the presence of 10–40 mM-Na^+ and 55–803 nM-Ca^{2+} in the internal solution, an increase of $[Ca^{2+}]_o$ from 0·1 to 0·5–20 mM or an increase of $[Na^+]_o$ from 30 to 50–140 mM induced an extra current associated with an increase in membrane conductance. The reversal potential of these extra currents was determined from an intersection of the current–voltage (*I–V*) relations obtained in the absence and presence of a Na^+–Ca^{2+} exchange blocker, Ni^{2+} (2 mM).

3. Ba^{2+} in the external solution failed to induce the extra current, but inhibited the background conductance having a reversal potential at around 0 mV. Thus, 1 mM-Ba^{2+} was added to all external solutions, so that a change in the background current was minimized during application of Ca^{2+} or Ni^{2+}.

4. The relation between $[Ca^{2+}]_o$ and amplitude of the Ca^{2+}-induced current was examined in the presence and absence of Ni^{2+}. Lineweaver–Burk analysis revealed that the action of Ni^{2+} on the extra current might be a mixed type of competitive and non-competitive inhibition.

5. During the application of Ca^{2+}, the Ca^{2+}-induced outward current decayed in a time-dependent manner, resulting in a shift of the *I–V* relations towards positive potentials. This current decay was inhibited by increasing the capacity of the internal Ca^{2+}-buffer, using BAPTA (1,2-bis(*o*-aminophenoxy)ethane-*N*,*N*,*N*′,*N*′-tetra-acetic acid) or higher concentrations of EGTA. The result indicates that $[Ca^{2+}]_i$, at least under the cell membrane, changes due to ion fluxes through the Na^+–Ca^{2+} exchange and that control of the ion concentrations within the cell is prerequisite for measuring the reversal potential of the Na^+–Ca^{2+} exchange.

6. The shift of both the holding current and the *I–V* relations during stimulation of the exchange was suppressed, when the membrane potential was clamped at the equilibrium potential of $3Na^+:1Ca^{2+}$ exchange. Under these conditions, the Ni^{2+}-

sensitive component of the Ca^{2+}- or Na^+-induced current showed reversal potentials which were in agreement with theoretical equilibrium potentials under the ionic conditions of 0·2–20 mM $[Ca^{2+}]_o$ and 30–140 mM $[Na^+]_o$.

7. We conclude that the external-Ca^{2+}- or external-Na^+-induced current is generated by the Na^+–Ca^{2+} exchange system and that the stoichiometry is $3Na^+:1Ca^{2+}$.

INTRODUCTION

The stoichiometry of the Na^+–Ca^{2+} exchange has been extensively investigated with tracer flux methods in squid axons (review by DiPolo & Beaugé, 1983), barnacle muscle fibres (Rasgado-Flores & Blaustein, 1987), cardiac membrane vesicles (review by Philipson, 1985) and intact cardiac strands (review by Langer, 1982). Many of these studies support the $3Na^+:1Ca^{2+}$ stoichiometry, thus the exchange is most probably electrogenic. Recently a membrane current component, which seems to be generated by the Na^+–Ca^{2+} exchange system, was recorded in retinal rod cells (Yau & Nakatani, 1984; Hodgkin, McNaughton & Nunn, 1987; Hodgkin & Nunn, 1987) and cardiac ventricular cells (Kimura, Noma & Irisawa, 1986; Kimura, Miyamae & Noma, 1987). If the pure Na^+–Ca^{2+} exchange current were to be isolated from other current components under known extra- and intracellular ionic conditions, stoichiometry of the Na^+–Ca^{2+} exchange can be determined directly by measuring its reversal potential, and analysis of the current response would give information on the exchange kinetics, as has been done for the Na^+–K^+ pump current (Nakao & Gadsby, 1986; Bahinski, Nakao & Gadsby, 1988). Further, the determination of reversal potentials at various external and internal Na^+ and Ca^{2+} concentrations would also provide information as to whether or not the stoichiometry is independent of the ion concentrations. Therefore, we extended the study of Kimura *et al.* (1986, 1987) in an attempt to obtain isolated Na^+–Ca^{2+} exchange current in single myocardial cells under various conditions.

Kimura *et al.* (1986, 1987) revealed that increases in external Na^+ or Ca^{2+} concentrations induced an increase of membrane conductance (Na^+- or Ca^{2+}-induced current) in internally perfused cardiac cells. This response was concluded to be generated by the Na^+–Ca^{2+} exchange system based on the following findings. The current response required the presence of both Na^+ and Ca^{2+} across the cell membrane, showed a Q_{10} value of 3·6–4·0, and was blocked by heavy metal ions or by removing free Ca^{2+} ions from the internal solution. The measurement of the reversal potential, however, was limited to a narrow range of $[Ca^{2+}]_o$, because the current–voltage relation of the Ca^{2+}-induced current showed a spontaneous shift of unknown origin. Since the measurement of the reversal potential is essential to determine whether this current is due to the Na^+–Ca^{2+} exchange system, we aimed first to clarify the mechanism of this time-dependent current decay and then to measure the reversal potential in wide ranges of Na^+ and Ca^{2+} concentrations, avoiding the time-dependent current change.

For isolation of the Na^+–Ca^{2+} exchange current, we adopted the subtraction method using Ni^{2+} for the blocking agent. It was previously reported that Ni^{2+} had no significant effect on background currents, but inhibited the Na^+–Ca^{2+} exchange

system fairly selectively (Kimura *et al.* 1987). We investigated the mechanism of Ni^{2+} action on the Na^+–Ca^{2+} exchange system using Lineweaver–Burk analysis.

The reversal potentials thus measured were in agreement with the theoretical equilibrium potential given by the stoichiometry of $3Na^+:1Ca^{2+}$. This ratio was constant in wide ranges of external Na^+ and Ca^{2+} concentrations and internal Ca^{2+} concentrations.

METHODS

Preparation of the cells

Single ventricular cells of guinea-pig heart were obtained with the enzymatic dissociation technique similar to that previously described (Powell, Terrar & Twist, 1980; Taniguchi, Kokubun, Noma & Irisawa, 1981; Isenberg & Klöckner, 1982). In brief, guinea-pigs of 300–400 g were anaesthetized with sodium pentobarbitone (20–50 mg/kg). Under artificial respiration, the chest was opened and the aorta was cannulated *in situ*. The heart was excised maintaining the Langendorff perfusion with control Tyrode solution and then perfused with Ca^{2+}-free Tyrode solution until the heart beat stopped. The perfusate was switched to a Ca^{2+}-free Tyrode solution containing collagenase (Sigma type I, 0·4 mg/ml) and trypsin inhibitor (Sigma, 0·4 mg/ml) for about 30 min at 37 °C. After this period, the heart was perfused with 'KB medium' (Isenberg & Klöckner, 1982). The left ventricle was then further dissected in a dish filled with KB medium. The dispersed ventricular cells were kept in KB medium before use.

Voltage-clamp and recording technique

Membrane currents of single ventricular cell were recorded using the whole-cell clamp technique, which was essentially the same as that described by Hamill, Marty, Neher, Sakmann & Sigworth (1981). To avoid the liquid junction potential and also to facilitate formation of the 'gigaohm seal', the pipette (tip diameter of about 3–4 μm) was first filled with Tyrode solution. After formation of the 'gigaohm seal', the pipette solution was replaced with an internal solution by the use of an intrapipette perfusion device (Soejima & Noma, 1984; Sato, Noma, Kurachi & Irisawa, 1985). A brief stronger suction was then applied to the inside of the pipette to rupture the patch membrane. Ramp voltage-clamp pulses (triangle wave; $dV/dt = \pm 0{\cdot}6 - 1$ V/s) were employed to obtain the current–voltage (I–V) relation. The I–V relation measured during the hyperpolarizing portion was used for analysis. The membrane capacitance (C_m) was measured by dividing the half-amplitude of the current jump at the turning points of the ramp pulse by the slope of the ramp pulse. The membrane current and voltage were recorded on videotapes (video recorder, TOSHIBA, A-700HFD, Tokyo, Japan) through a PCM converter (SONY, PCM-501ES, Tokyo, Japan) for later computer analysis (NEC, PC98 XA, Tokyo, Japan).

Solutions

The control Tyrode solution contained (in mM): NaCl, 140; KCl, 5·4; $MgCl_2$, 0·5; $CaCl_2$, 1·8; NaH_2PO_4, 0·33; glucose, 11·0; HEPES, 5·0 (pH = 7·4 with NaOH). The main composition of external solutions used for measurements of the Na^+- or Ca^{2+}-induced current was (in mM): NaCl, 140; $MgCl_2$, 2·0; HEPES, 5·0 (pH = 7·4 with CsOH). In low-Na^+ external solutions, NaCl was replaced with equimolar LiCl. When changing the external Ca^{2+} concentration, desired amounts of $CaCl_2$ were added. To suppress membrane current components other than the Na^+–Ca^{2+} exchange current, the following blockers were added to the external solution: 20 μM-ouabain to block the Na^+–K^+ pump, 1·0 mM-$BaCl_2$ to block K^+ channels and 1·0 μM-nicardipine-HCl to block Ca^{2+} channels. The action of nicardipine did not show a significant voltage dependence (Terada, Kitamura & Kuriyama, 1987).

Nicardipine-HCl was a gift from Yamanouchi Pharmaceutical Co. Ltd, Tokyo, Japan.

The composition of internal solutions is listed in Table 1. Tetraethylammonium chloride (TEA, 20 mM) was added to the internal solution to block K^+ channels. The internal solutions also contained high concentrations of EGTA or BAPTA (1,2-bis(*o*-aminophenoxy)ethane-*N*,*N*,*N*′,*N*′-tetraacetic acid). The concentrations of internal free Ca^{2+} and free Mg^{2+} were adjusted by adding appropriate amounts of $CaCl_2$ and $MgCl_2$ to these BAPTA or EGTA buffers. The free Ca^{2+}

concentration was calculated by using Fabiato & Fabiato's equations (1979) with the correction by Tsien & Rink (1980) and with dissociation constants of BAPTA (Tsien, 1980). All experiments were performed at 36–37 °C.

TABLE 1. Composition of internal solutions

Free Ca^{2+} (nM)	153	153	153	153	253	803	55
BAPTA (mM)	42	42	—	10	30	30	—
EGTA (mM)	—	—	42	—	—	—	42
$CaCl_2$ (mM)	18·4	18·4	29·0	4·4	16·9	24·1	20
$MgCl_2$ (mM)	13·2	13·2	13·0	11·7	12·3	11·8	1·3
NaOH (mM)	15	—	—	—	—	—	30
Aspartate (mM)	42	42	42	42	42	42	42
K_2ATP (mM)	10	10	10	10	10	10	10
Na_2creatine-phosphate (mM)	5·0	5·0	5·0	5·0	5·0	5·0	5·0
TEA-Cl (mM)	20	20	20	20	20	20	20
Figure	1	3,4	2,7,9	3,4	12	10	5

BAPTA; 1,2-bis(*o*-aminophenoxy)ethane-*N*,*N*,*N*′,*N*′-tetraacetic acid, potassium salt (Dotite); EGTA; ethyleneglycol-bis(*β*-aminoethyl ether)*N*,*N*,*N*′,*N*′-tetraacetic acid (Sigma). Free Mg^{2+} concentration was adjusted to 1·5–1·6 mM except for the case in Fig. 5 (10 μM). The pH was adjusted to 7·4 with 5·0 mM-HEPES–CsOH.

It was considered that concentrations of the intracellular ions may not exactly be equal to those of ions in the pipette solution, because diffusion of ions through the pipette tip might be limited. In this paper $[Na^+]_i$ and $[Ca^{2+}]_i$ refer to the Na^+ concentration and the free Ca^{2+} concentration in the pipette solution, respectively. The equilibrium potential of the Na^+–Ca^{2+} exchange, $E_{Na,Ca}$, is based on $3Na^+:1Ca^{2+}$ stoichiometry unless otherwise stated (Mullins, 1977):

$$E_{Na,Ca} = 3E_{Na} - 2E_{Ca},$$

where E_{Na} and E_{Ca} are equilibrium potentials of Na^+ and Ca^{2+} across the membrane given by the Nernst equation.

RESULTS

Effect of Ba^{2+} on the background current

The Na^+–Ca^{2+} exchange current was isolated as a Ni^{2+}-sensitive current component, assuming that Ni^{2+} selectively blocks the Na^+–Ca^{2+} exchange under the present experimental condition, where most of the voltage-dependent ionic channels and electrogenic Na^+–K^+ pump were blocked (see Methods). However, even under this condition, isolation of the Na^+–Ca^{2+} exchange current from remaining background currents was still hampered by a change in the background current. When the Na^+–Ca^{2+} exchange was activated by increasing $[Ca^{2+}]_o$, or was blocked by applying Ni^{2+}, the background current was also affected. This situation was much improved by a continuous application of Ba^{2+}. Ba^{2+} effectively blocked the background current without showing any sign of stimulation of the Na^+–Ca^{2+} exchange (see also Tibbits & Philipson, 1985).

Figure 1 shows the effect of Ba^{2+} on the background current. The *I*–*V* relations were obtained by ramp pulses in the presence of 1, 2, 5 and 10 mM-external Ba^{2+}. The slope conductance decreased with increases of the Ba^{2+} concentration. The reversal potential of the Ba^{2+}-sensitive current seemed to be about 0 mV. Furthermore, the

depressing effect of Ba^{2+} at positive and negative potentials was almost symmetrical around the reversal potential, suggesting that Ba^{2+} inhibited the background conductance of a non-specific ionic nature.

The effect of Ni^{2+} on the background current in the presence of 1 mM-Ba^{2+} can be seen in Fig. 7*B*. When $[Ca^{2+}]_o$ is 0·1 mM, at which concentration the Na^+–Ca^{2+}

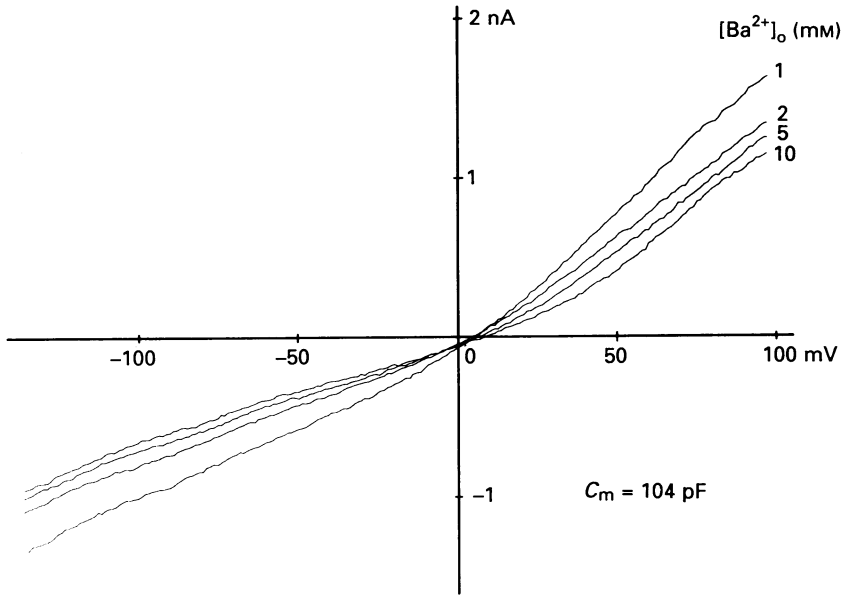

Fig. 1. *I–V* relations obtained by ramp pulses in the presence of external 1, 2, 5 and 10 mM-Ba^{2+}. Each *I–V* relation shown is the average of four *I–V* relations at each Ba^{2+} concentration. The Ba^{2+} concentrations (in mM) are indicated to the right of each trace. Ionic conditions were 25 mM $[Na^+]_i$, 153 nM $[Ca^{2+}]_i$, 140 mM $[Na^+]_o$ and 0·1 mM $[Ca^{2+}]_o$. The holding potential was −35 mV. C_m indicates the capacitance of the cell.

exchange operates little (see below), the *I–V* relations in the absence and presence of 2 mM-Ni^{2+} were almost superimposable. This finding indicates that Ni^{2+} had insignificant effects on the background current which was already suppressed by Ba^{2+}. Thus, we attempted to separate the Na^+–Ca^{2+} exchange current using Ni^{2+}. All of the following experiments included 1 mM-Ba^{2+} in the external solution.

Shift of apparent reversal potential

In addition to the above contaminating background current, measurement of the reversal potential met another complication. Figure 2 shows representative records of a time-dependent shift of the *I–V* curve during sustained activation of the Ca^{2+}-induced current. The holding potential was set at +38 mV, a value equal to the equilibrium potential of the $3Na^+:1Ca^{2+}$ exchange ($E_{Na,Ca}$ in the presence of 10 mM $[Na^+]_i$, 153 nM $[Ca^{2+}]_i$, 140 mM $[Na^+]_o$ and 0·1 mM $[Ca^{2+}]_o$). Increase of $[Ca^{2+}]_o$ from 0·1 to 10 mM induced an outward current ($E_{Na,Ca} = -85$ mV at 10 mM $[Ca^{2+}]_o$), but its amplitude decreased with time even in the sustained presence of 10 mM $[Ca^{2+}]_o$. On

switching to 0·1 mM $[Ca^{2+}]_o$, the holding current showed an undershoot, which thereafter levelled off to the control level.

The *I–V* relations marked by *a* to *f* in Fig. 2 were recorded every 6 s by ramp pulses during the application of 10 mM $[Ca^{2+}]_o$. If the background current is approximated by the *I–V* relation obtained at 0·1 mM $[Ca^{2+}]_o$ (bold curve in Fig. 2), then the finding

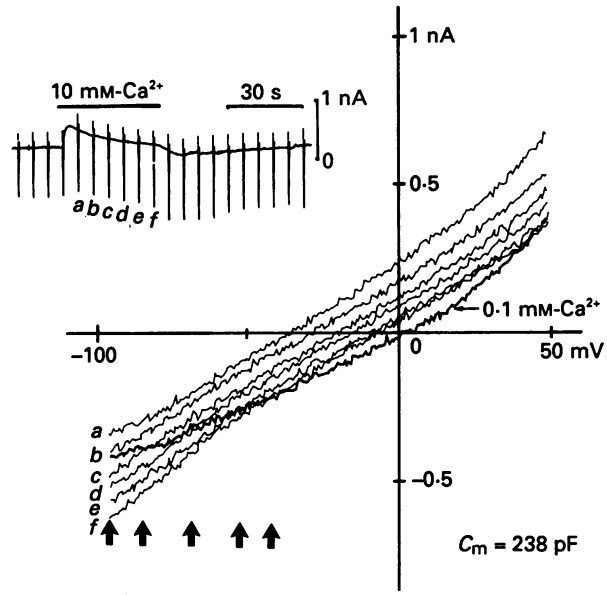

Fig. 2. Consecutive *I–V* relations obtained by ramp pulses during application of 10 mM $[Ca^{2+}]_o$ (*a–f*) under conditions of 10 mM $[Na^+]_i$, 153 nM $[Ca^{2+}]_i$ and 140 mM $[Na^+]_o$. The control *I–V* relation at 0·1 mM $[Ca^{2+}]_o$ is also shown (bold curve). The inset shows the chart record of current, and the current traces indicated by *a–f* are shown in the graph. Holding potential was +38 mV. Ramp pulses were applied every 6 s. The external solution was changed from 0·1 to 10 mM $[Ca^{2+}]_o$ for a period indicated above the current trace. Arrows in the graph indicate intersecting voltage of the control *I–V* relation and the other *I–V* relations (*a–f*).

indicated that the reversal potential shifted from a potential more negative than −100 mV to about −40 mV, as indicated by the arrows. One explanation for this finding is to assume that Ca^{2+} accumulation and Na^+ depletion occurred within the cell, resulting from ion fluxes through the Na^+–Ca^{2+} exchanger.

Intracellular Ca^{2+} accumulation and Na^+ depletion

Any rise in the intracellular concentration of free Ca^{2+} would be inhibited by increasing the capacity of the Ca^{2+} buffer in the internal solution. In the experiment shown in Fig. 3, we compared the Ca^{2+}-induced currents obtained at 10 mM- (*A*) and 42 mM-BAPTA (*B*), an agent which was expected to take up and release Ca^{2+} faster than EGTA (Tsien, 1980). At the higher concentration of BAPTA, decay of the Ca^{2+}-induced current was slower and the *I–V* relations shifted less extensively than at 10 mM-BAPTA at the holding potential of +38 mV (= $E_{Na, Ca}$ at 0·1 mM $[Ca^{2+}]_o$). Moreover, changes in the *I–V* curves observed at 42 mM-BAPTA were clearly

smaller than those observed with equimolar EGTA (see Fig. 2). These results are in line with the view regarding Ca^{2+} accumulation.

The shift of *I–V* relations will also be suppressed by minimizing the continuous Ca^{2+} influx using a holding potential close to $E_{Na,Ca}$. This was the case as shown in the lower part of Fig. 3, where the holding potential was set at −85 mV (= $E_{Na,Ca}$

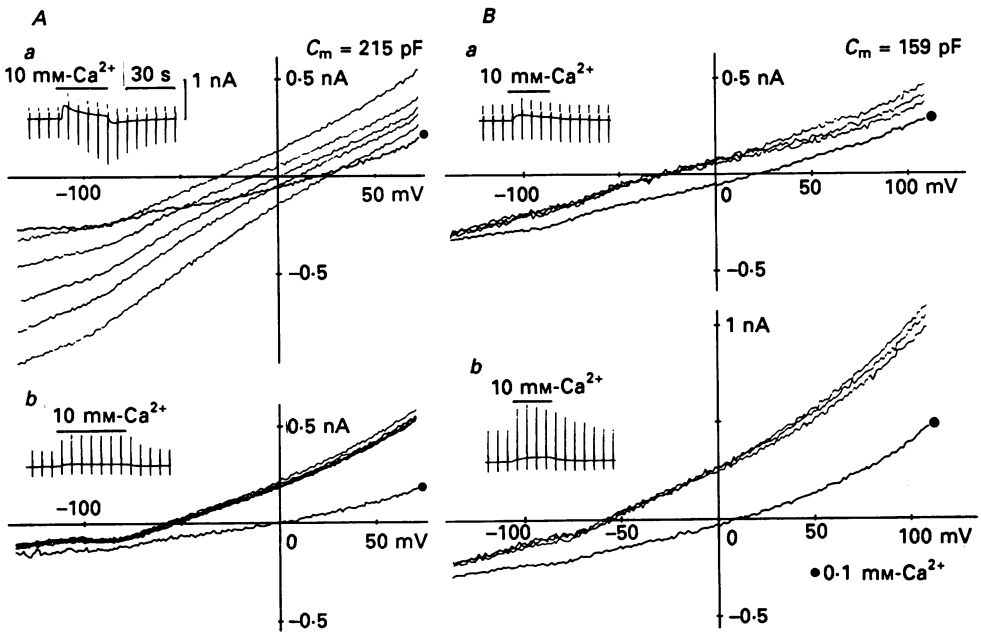

Fig. 3. Effect of holding potential and high concentrations of internal BAPTA on the shift of *I–V* relations. *I–V* relations were obtained by ramp pulses during exposure to 10 mM-$[Ca^{2+}]_o$ with a holding potential of +38 (*a*) or −85 mV (*b*). *A* shows the responses with 10 mM-internal BAPTA. *B* shows those with 42 mM-internal BAPTA in a different cell. Ionic conditions were 10 mM $[Na^+]_i$, 153 nM $[Ca^{2+}]_i$ and 140 mM $[Na^+]_o$. The control *I–V* relation at 0·1 mM $[Ca^{2+}]_o$ is shown in each case (●). The insets are chart records of the current under each condition. The ramp pulses were given every 6 s.

at 10 mM $[Ca^{2+}]_o$) about 1 min before the application of 10 mM $[Ca^{2+}]_o$. The shift of *I–V* relations was small compared with that observed at the holding potential of +38 mV in both cases of 10 and 42 mM-BAPTA. These results support the view that the time-dependent shift of the *I–V* relations was caused by Ca^{2+} accumulation, and probably also by Na^+ depletion within the cell. The outward shift of the holding current in response to 10 mM $[Ca^{2+}]_o$ observed at −85 mV is not due to the exchange current, rather it probably reflects changes in background conductance (see Discussion).

Our proposal was further tested by recording the decay of the Ca^{2+}-induced current during the voltage jump. As shown in Fig. 4*A*, in the presence of 10 mM $[Ca^{2+}]_o$ the outward current induced by a depolarizing pulse decayed exponentially, and repolarization induced a large undershoot which exponentially levelled off to the control holding current level. These time-dependent current changes were not

observed when $[Ca^{2+}]_o$ was lower than 0·1 mM. The time constants on depolarization and repolarization were 5·3 s and 4·1 s, respectively. After the pipette solution containing 10 mM-BAPTA was replaced with that containing 42 mM-BAPTA, decay of the current response became slower; the time constants were 11·3 s on depolarization and 22·7 s on repolarization. On average, the time constants obtained with 10 mM-BAPTA were 5·9 ± 0·9 s (mean ± S.D.) on depolarization and 3·7 ± 0·4 s on

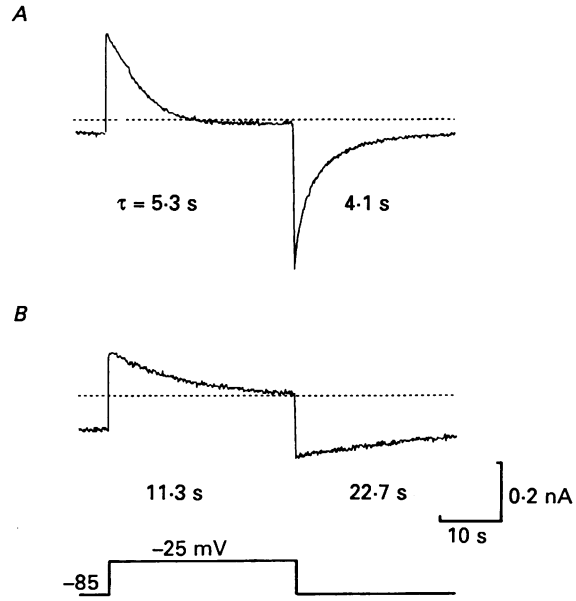

Fig. 4. Current traces on voltage jump in 10 mM-internal BAPTA (*A*) and 42 mM-internal BAPTA (*B*) under the same ionic conditions as in Fig. 3 ($[Ca^{2+}]_o$ = 10 mM). Depolarizing clamp pulse was applied from a holding potential of −85 to −25 mV for 30 s. Time constants of the current decay on depolarization (left) and on repolarization (right) are shown for each trace.

repolarization (n = 3) and those obtained with 42 mM-BAPTA were 29·8 ± 10·3 s and 98·3 ± 33·4 s (n = 4), respectively. We conclude that $[Ca^{2+}]_i$ changes with time even in the presence of a strong Ca^{2+}-buffering system in the internal solution, when the Na^+–Ca^{2+} exchange is operative. It should be noted that such changes in ion concentrations may not necessarily occur in the entire cell, rather they may be confined to some restricted spaces under the membrane which are more directly linked to the function of the exchanger.

Mechanism of Ni^{2+} action on Na^+–Ca^{2+} exchange system

Before separating the Na^+–Ca^{2+} exchange current using Ni^{2+}, we conducted the Lineweaver–Burk analysis to get an insight into the mechanism of Ni^{2+} action on the Na^+–Ca^{2+} exchanger. The dose–response curve for the Ca^{2+}-induced outward current was measured in the absence and presence of Ni^{2+}. The holding potential was set at −100 mV, a value equal to $E_{Na,Ca}$, in the presence of 140 mM $[Na^+]_o$, 0·1 mM $[Ca^{2+}]_o$, 40 mM $[Na^+]_i$ and 55 nM $[Ca^{2+}]_i$. The increases of $[Ca^{2+}]_o$ from 0·1 mM to various

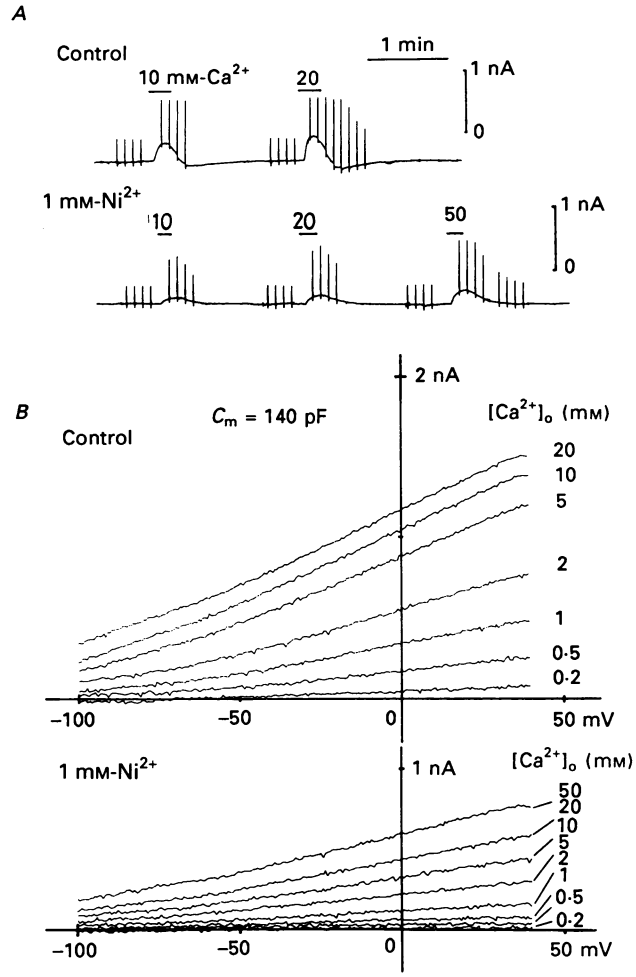

Fig. 5. Effect of Ni^{2+} on the Ca^{2+}-induced current. *A*, current records from a cell on changing $[Ca^{2+}]_o$ from 0·1 mM to higher concentrations in absence (Control) and presence of 1 mM-Ni^{2+}. Current responses (spikes) during ramp pulses are superimposed. Various $[Ca^{2+}]_o$ were applied for the time indicated by bars, above which $[Ca^{2+}]_o$ is shown. Ionic conditions were 40 mM $[Na^+]_i$, 55 nM $[Ca^{2+}]_i$ and 140 mM $[Na^+]_o$. Holding potential was −100 mV. *B*, *I–V* relations of the difference current between current at 0·1 mM $[Ca^{2+}]_o$ and that at each higher $[Ca^{2+}]_o$ obtained in absence (control) and presence of 1 mM-Ni^{2+}. Data from the experiment shown in *A*. Subtraction was made between the *I–V* relation obtained at the peak of each response to higher $[Ca^{2+}]_o$ and that at 0·1 mM $[Ca^{2+}]_o$. Ca^{2+} concentrations (in mM) are shown on the right of each trace.

concentrations induced an outward current in a dose-dependent manner. The *I–V* relations were measured with ramp pulses and those obtained at the peak of the Ca^{2+}-induced current response were used for analysis, assuming that changes in $[Ca^{2+}]_i$ and $[Na^+]_i$ were negligibly small at this point. The *I–V* curves in Fig. 5*B* were obtained by subtracting the control *I–V* relation at 0·1 mM $[Ca^{2+}]_o$ from those obtained at the peak of each response. The same cell was then superfused

continuously with external solutions containing 1 mM-Ni^{2+}, and the measurement of the *I–V* relations was repeated at each $[Ca^{2+}]_o$ (Fig. 5*A*, lower trace). The lower panel of Fig. 5*B* shows the *I–V* curves of the Ca^{2+}-induced current obtained under the influence of Ni^{2+}.

The dose–response relationship was evaluated in Fig. 6 by plotting the amplitude of the Ca^{2+}-induced outward current at +35 mV (Fig. 5), where the Ca^{2+}-induced

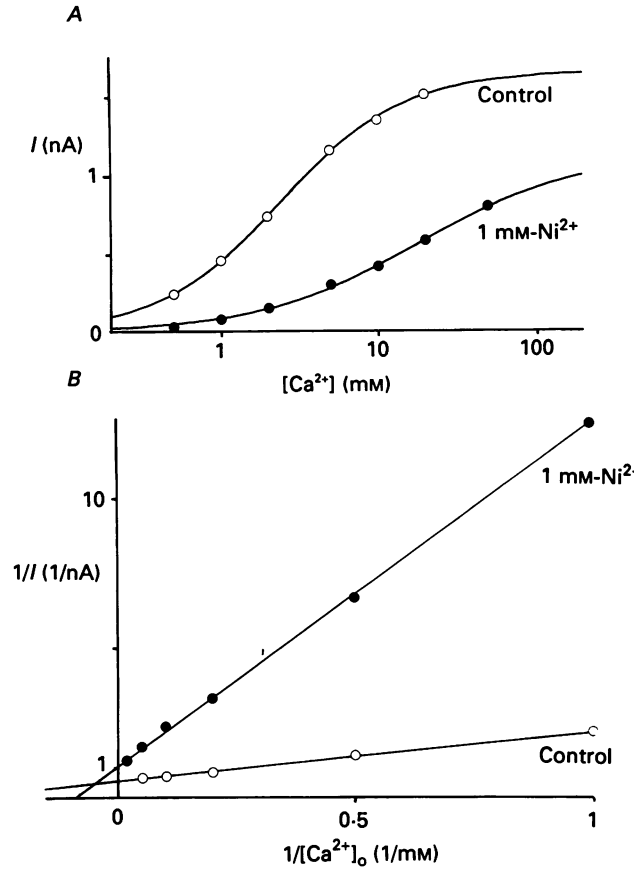

Fig. 6. *A*, dose–response relations of the Ca^{2+}-induced current in the absence (○) and presence (●) of 1 mM-Ni^{2+}. The current amplitudes at +35 mV in Fig. 5*B* are plotted against $[Ca^{2+}]_o$ on a semilogarithmic scale. Continuous lines are fitted by the Hill equation. *B*, Lineweaver–Burk analysis of Ni^{2+} action on the Ca^{2+}-induced current. Data in *A* are replotted on a double-reciprocal scale. The straight lines were obtained by the least-squares method.

current should be substantially larger than the contaminating background current. We did not make an attempt to measure directly the maximum current response, since very high doses of external Ca^{2+} might cause unknown effects on the membrane other than stimulating the Na^+–Ca^{2+} exchange, such as a surface potential change or a conductance change due to rapid accumulation of Ca^{2+} inside. In the Lineweaver–Burk plot shown in Fig. 6*B*, the data were well fitted with a straight line

in both the absence and presence of Ni^{2+}. This finding agrees with the previous report that the Hill coefficient is nearly 1 (Kimura *et al.* 1987). The graphic evaluation in the Lineweaver–Burk plot suggests that the inhibitory action of Ni^{2+} is a mixed type of competitive and non-competitive inhibition.

The parameters used for the best curve fitting obtained in four cells are shown in Table 2. Ni^{2+} increased the half-maximal Ca^{2+} concentration, K_m, from $2{\cdot}6 \pm 0{\cdot}5$ to

TABLE 2. Effect of Ni^{2+} on the outward current

Cell no.	$K_{m(c)}$ (mM/l)	$K_{m(Ni)}$ (mM/l)	$V_{max(c)}$ (nA)	$V_{max(Ni)}$ (nA)	$V_{max(Ni)}/V_{max(c)}$ (%)
1	3·40	8·08	1·96	0·58	29·6
2	2·15	15·92	1·61	1·04	64·6
3	2·46	3·76	3·05	0·68	22·3
4	2·54	2·53	2·18	0·32	14·7
Mean ± S.D.	2·64 ± 0·46	7·57 ± 5·2			32·8 ± 19·1

$K_{m(c)}$ and $K_{m(Ni)}$ are the half-maximal Ca^{2+} concentrations in the absence and presence of 1 mM-Ni^{2+}, respectively. $V_{max(c)}$ and $V_{max(Ni)}$ are the maximum current responses in the absence and presence of Ni^{2+}, respectively. Current responses to the external Ca^{2+} were measured at +35 mV.

$7{\cdot}6 \pm 5{\cdot}2$ mM and decreased the maximum current response, V_{max}, by $32{\cdot}8 \pm 19{\cdot}1$ %. Ni^{2+} may bind to the Na^+–Ca^{2+} exchanger at the same site as does Ca^{2+} and also at another allosteric site whose association with Ni^{2+} depresses the carrier function.

To test voltage dependence of the Ni^{2+} action, the above analysis was also made at −50 and 0 mV. The Lineweaver–Burk analysis at each potential (not shown) revealed essentially the same result as in Fig. 6*B*. Furthermore, close inspection of the *I–V* relations such as are shown in Fig. 5*B* revealed that for each $[Ca^{2+}]_o$ Ni^{2+} reduced the Ca^{2+}-induced current by a nearly constant ratio at any potential examined. Therefore, it was concluded that the action of Ni^{2+} on Na^+–Ca^{2+} exchange system is voltage independent.

Relationship between $[Ca^{2+}]_o$ and the reversal potential

To measure the reversal potential of the Ca^{2+}-induced current at fixed $[Na^+]_i$, $[Ca^{2+}]_i$ and $[Na^+]_o$, the holding potential was changed to a value matching the $E_{Na,Ca}$ for the new $[Ca^{2+}]_o$ immediately after starting the perfusion of the solution with this $[Ca^{2+}]_o$. With this procedure, the holding current at the new level did not appreciably change during the application of high $[Ca^{2+}]_o$, as expected. An example of such experiments is shown in Fig. 7. In this experiment $[Na^+]_i$, $[Ca^{2+}]_i$ and $[Na^+]_o$ were 10 mM, 153 nM and 140 mM, respectively. After measuring *I–V* curves using four ramp pulses, the cell was superfused with solution containing 2 mM-Ni^{2+}. Although Ni^{2+} did not change the holding current, the amplitude of the current deflection induced by the ramp pulses decreased.

In Fig. 7*B*, *I–V* relations obtained in the same one cell before and during the application of Ni^{2+} were demonstrated for each $[Ca^{2+}]_o$. The four successive *I–V* relations were superimposable both in the absence and presence of Ni^{2+}. The two families of *I–V* curves (filled circles indicate currents in the presence of Ni^{2+}) intersected at a certain membrane potential (arrows). At 0·1 mM $[Ca^{2+}]_o$, the *I–V*

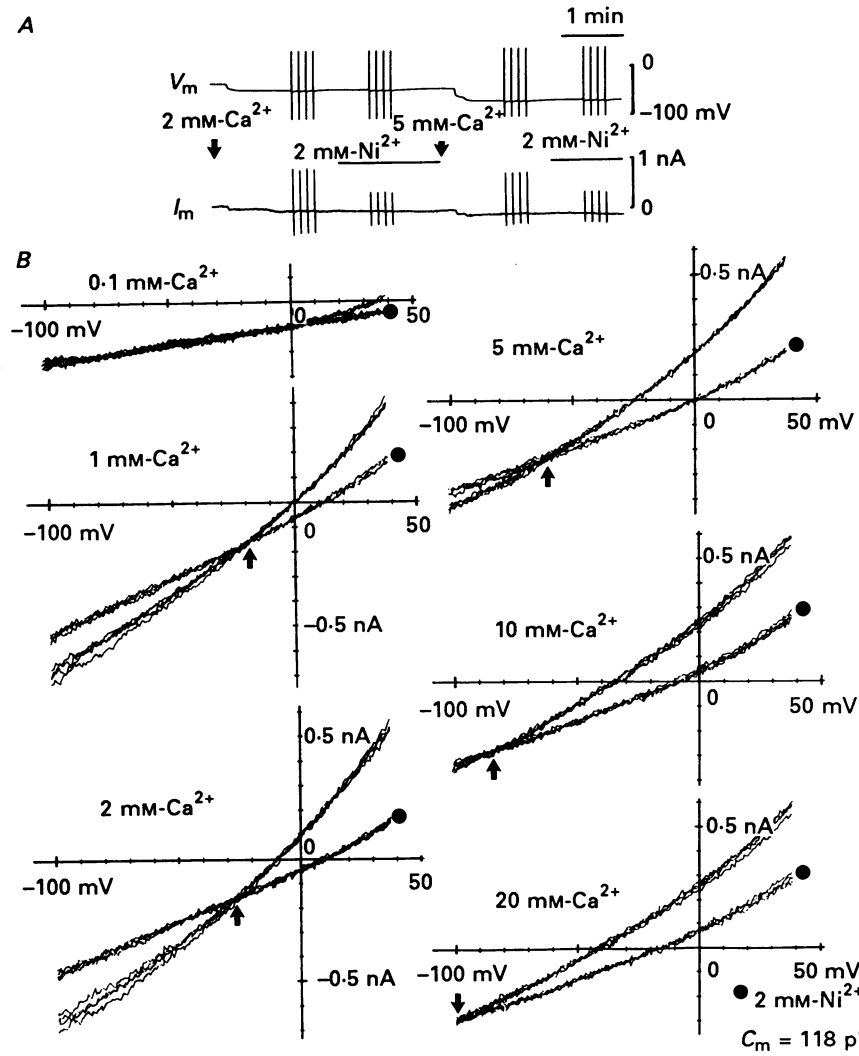

Fig. 7. Measurement of reversal potential of Ca^{2+}-induced current. *A*, chart record of voltage (top trace) and current (bottom trace). The holding potential and $[Ca^{2+}]_o$ were initially −23 mV and 1 mM, respectively. At the first arrow 2 mM-Ca^{2+} was applied, and subsequently the holding potential was shifted to −42 mV, the predicted $E_{Na,Ca}$ at 2 mM $[Ca^{2+}]_o$. The *I–V* relation was determined four times (spikes) with ramp pulses at this $[Ca^{2+}]_o$, and then 2 mM-Ni^{2+} was added (bar) with determination of the *I–V* relation. At the second arrow $[Ca^{2+}]_o$ was increased to 5 mM and Ni^{2+} was omitted, and the above protocol was repeated with the predicted $E_{Na,Ca}$ for 5 mM $[Ca^{2+}]_o$, −66 mV. Other ionic conditions were 10 mM $[Na^+]_i$, 153 nM $[Ca^{2+}]_i$ and 140 mM $[Na^+]_o$. *B*, *I–V* relations obtained at various $[Ca^{2+}]_o$ in the absence and presence (●) of 2 mM-Ni^{2+}. Data from experiments shown in *A*. For each curve, four consecutive *I–V* relations were superimposed. Arrows indicate intersection of the two families of *I–V* relations.

relations before and during superfusing Ni^{2+} were almost superposable, thereby indicating that the Na^+–Ca^{2+} exchange system was not activated. As $[Ca^{2+}]_o$ was increased, the potential of the intersection became more negative.

When the slope conductance was compared between different *I–V* curves recorded in the presence of Ni^{2+} (filled circles), the background slope conductance was usually minimum at the beginning, increased in the course of the experiment and reached a

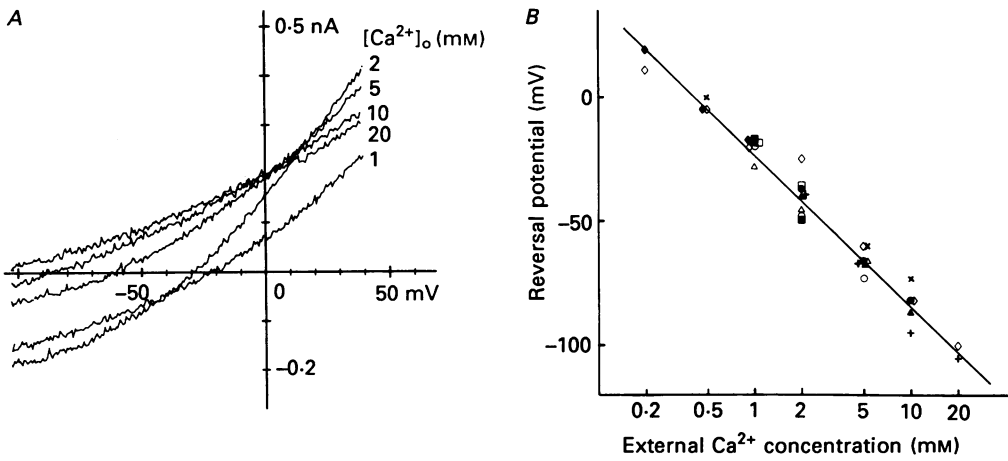

Fig. 8. *A*, *I–V* relations of Ni^{2+}-sensitive current. The difference between average *I–V* relations obtained in the absence and presence of 2 mM-Ni^{2+} is plotted for various $[Ca^{2+}]_o$. Data from experiment shown in Fig. 7. $[Ca^{2+}]_o$ values are indicated on the right of each trace. *B*, reversal potential of Ni^{2+}-sensitive current as a function of $[Ca^{2+}]_o$. Data from eleven cells are plotted against $[Ca^{2+}]_o$ on a semilogarithmic scale. The straight line shows theoretical equilibrium potential of Na^+–Ca^{2+} exchange given by $3Na^+:1Ca^{2+}$ exchange. Different symbols indicate different cells.

new steady level. The smallest slope conductance of the *I–V* relations at 0·1 mM $[Ca^{2+}]_o$ was recorded at the beginning of the experiment and recordings at 1 mM $[Ca^{2+}]_o$ were followed. However, the slope of *I–V* relations in the presence of Ni^{2+} decreased, as $[Ca^{2+}]_o$ was increased from 1 to 2 mM. We assumed that Ca^{2+}, like Ba^{2+} (refer to Fig. 1), may decrease the background conductance.

The *I–V* relations for the Ni^{2+}-sensitive current were calculated as the difference between averages of each family of records in the absence and presence of Ni^{2+} and are demonstrated in Fig. 8*A*. The *I–V* curves showed an exponential slope at potentials positive to the reversal potential, and a tendency towards saturation of the inward current at potentials negative to the reversal potential. The slope of the outward current increased as $[Ca^{2+}]_o$ was increased from 1 to 2 mM, because of a more extensive activation of the exchange. Further increases of $[Ca^{2+}]_o$ up to 20 mM, however, decreased the slope, probably because the Ni^{2+} action competed with that of Ca^{2+}, resulting in a less inhibition of the exchange at higher $[Ca^{2+}]_o$.

This type of experiment was successfully performed in eleven cells. In seven out of these eleven cells, there was no clear intersection, as shown in Fig. 9. In such cases, the null point (arrow) of the Ni^{2+}-sensitive outward current was regarded as the reversal.

The reversal potentials thus measured were plotted against $[Ca^{2+}]_o$ on a semilogarithmic scale in Fig. 8*B*. The straight line indicates the theoretical equilibrium potential for the $3Na^+:1Ca^{2+}$ exchange, calculated from the ion compositions in both external and internal solutions. The values measured were in good agreement with the theoretical ones in the $[Ca^{2+}]_o$ range examined.

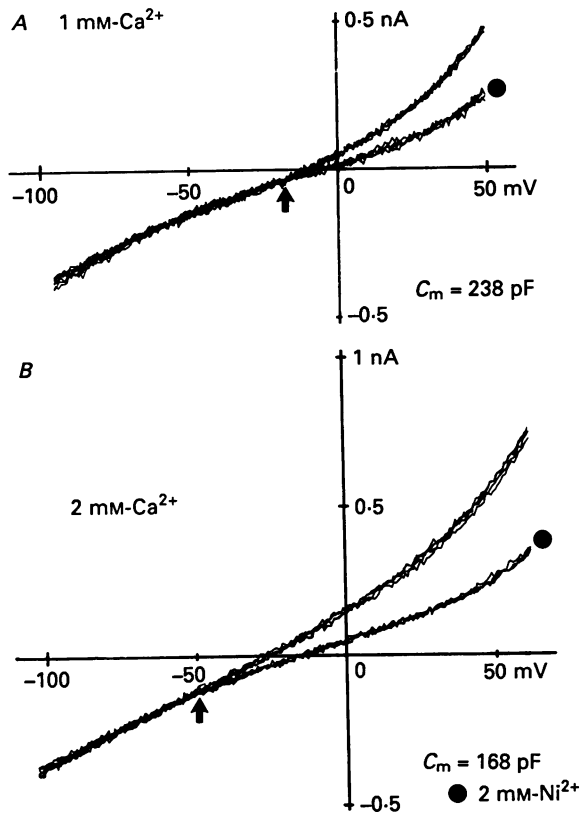

Fig. 9. *I–V* relations at 1 mM $[Ca^{2+}]_o$ (*A*) and 2 mM $[Ca^{2+}]_o$ (*B*) obtained before and during (●) application of 2 mM-Ni^{2+}. Experimental protocol and conditions were the same as in Fig. 7. *A* and *B* show data from different cells. Arrow indicates 'reversal' of the Ni^{2+}-sensitive current estimated in these cases. See text.

As for cases without a clear current intersection (Fig. 9), it was hypothesized that the internal Ca^{2+} concentration of 153 nM was too low for internal Ca^{2+}-binding sites to be occupied by Ca^{2+}, so that the inward current component was not sufficiently activated.

The reversal potential of Na^+–Ca^{2+} exchange current at high $[Ca^{2+}]_i$

To test the above hypothesis, the same protocol as in Fig. 7 was repeated, using an internal solution containing 803 nM $[Ca^{2+}]_i$. The results, which are shown in Figs 10 and 11, are similar to those obtained in Figs 7 and 8. As expected, the *I–V* relations before and after Ni^{2+} showed a clear intersection in all five cells examined. This

finding is consistent with the hypothesis that a $[Ca^{2+}]_i$ more than at least 153 nM is needed for the Na^+–Ca^{2+} exchanger to generate the inward Na^+–Ca^{2+} exchange current.

The *I–V* relations of the Ni^{2+}-sensitive current obtained using 803 nM $[Ca^{2+}]_i$ are shown in Fig. 11*A*. In this series of experiments, the finding of the exponential or linear increase of the outward current in Fig. 8 was extended up to +100 mV. The

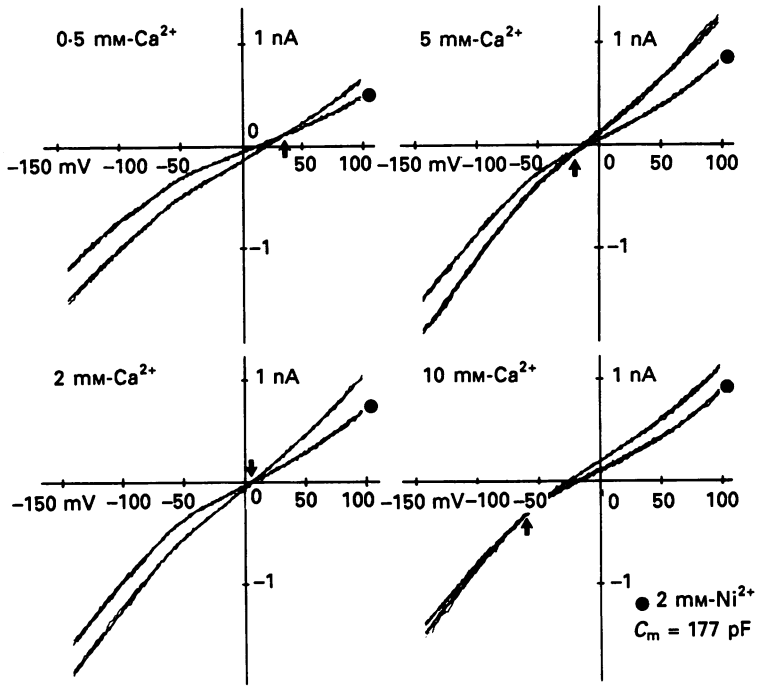

Fig. 10. *I–V* relations at various $[Ca^{2+}]_o$ obtained before and during (●) application of 2 mM-Ni^{2+}. Ionic conditions and experimental protocol were the same as those in Fig. 7 except that $[Ca^{2+}]_i$ was 803 nM. Four successive *I–V* relations obtained before and during application of Ni^{2+} are superimposed for each $[Ca^{2+}]_o$. Arrows indicate intersection of the two families of *I–V* relations.

tendency of saturation of the inward current was also observed as in Fig. 8*A*, but no sign of decrease was observed even when the membrane was hyperpolarized up to −140 mV. This result is different from that predicted for one type of Na^+–Ca^{2+} exchange model (Eisner & Lederer, 1985).

The reversal potentials obtained using 803 nM $[Ca^{2+}]_i$ solution in five cells are demonstrated in Fig. 11*B*. The reversal potentials here again agreed well with the theoretical values given by $3Na^+$:$1Ca^{2+}$ stoichiometry. It was concluded that the stoichiometry was constant in a range of $[Ca^{2+}]_o$ from 0·2 to 20 mM and of $[Ca^{2+}]_i$ from 153 to 803 nM.

Relationship between $[Na^+]_o$ and the reversal potential

The $E_{Na,Ca}$ is also a function of $[Na^+]_o$, which can be controlled under the present experimental conditions. The $[Na^+]_o$ was varied between 30 and 140 mM by

substituting Na^+ with equimolar Li^+. The reversal potentials of the Ni^{2+}-sensitive component of the Na^+-induced current were measured using the same protocol as used for the Ca^{2+}-induced current (Figs 7 and 10). The four consecutive I–V relations at 30, 50, 70 and 140 mM $[Na^+]_o$ before and during superfusing 2 mM-Ni^{2+} are

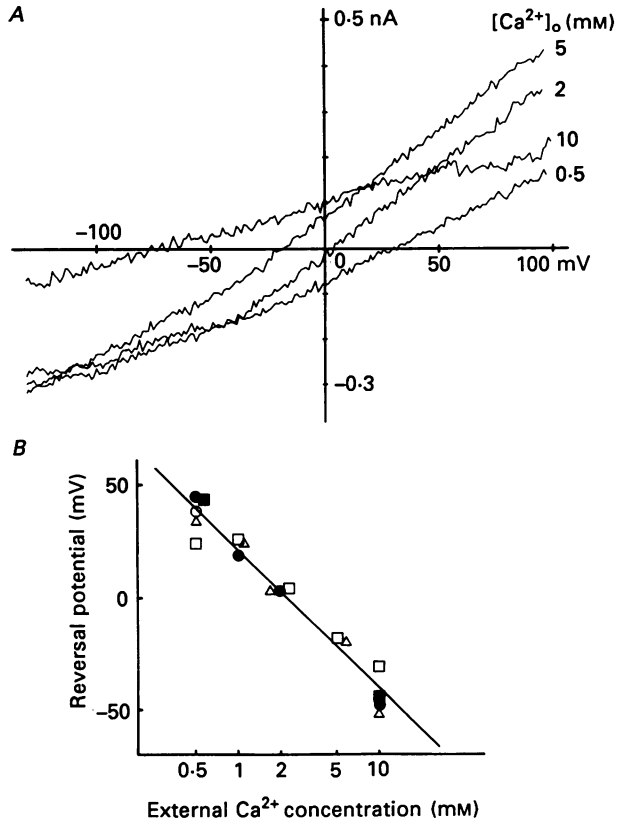

Fig. 11. A, 1–V relations of Ni^{2+}-sensitive current obtained at 803 nM $[Ca^{2+}]_i$. Data from experiment shown in Fig. 10. Currents are drawn in the same manner as for Fig. 8A. B, reversal potential of Ni^{2+}-sensitive current as a function of $[Ca^{2+}]_o$, obtained at 803 nM $[Ca^{2+}]_i$. Data from five cells are plotted against $[Ca^{2+}]_o$ on a semilogarithmic scale. The straight line shows theoretical equilibrium potential of the Na^+–Ca^{2+} exchange given by the $3Na^+$:$1Ca^{2+}$ exchange. Different symbols indicate different cells.

demonstrated in Fig. 12A. These two groups of the I–V relations intersected consistently in all the cells examined ($n = 4$).

Figure 12B summarizes such measurements of the reversal potential with the $E_{Na,Ca}$ given by the stoichiometry of $3Na^+$:$1Ca^{2+}$ exchange. The agreement of the data with the theoretical values indicates that the stoichiometry of $3Na^+$:1 Ca^{2+} is fixed in a range of $[Na^+]_o$ from 30 to 140 mM.

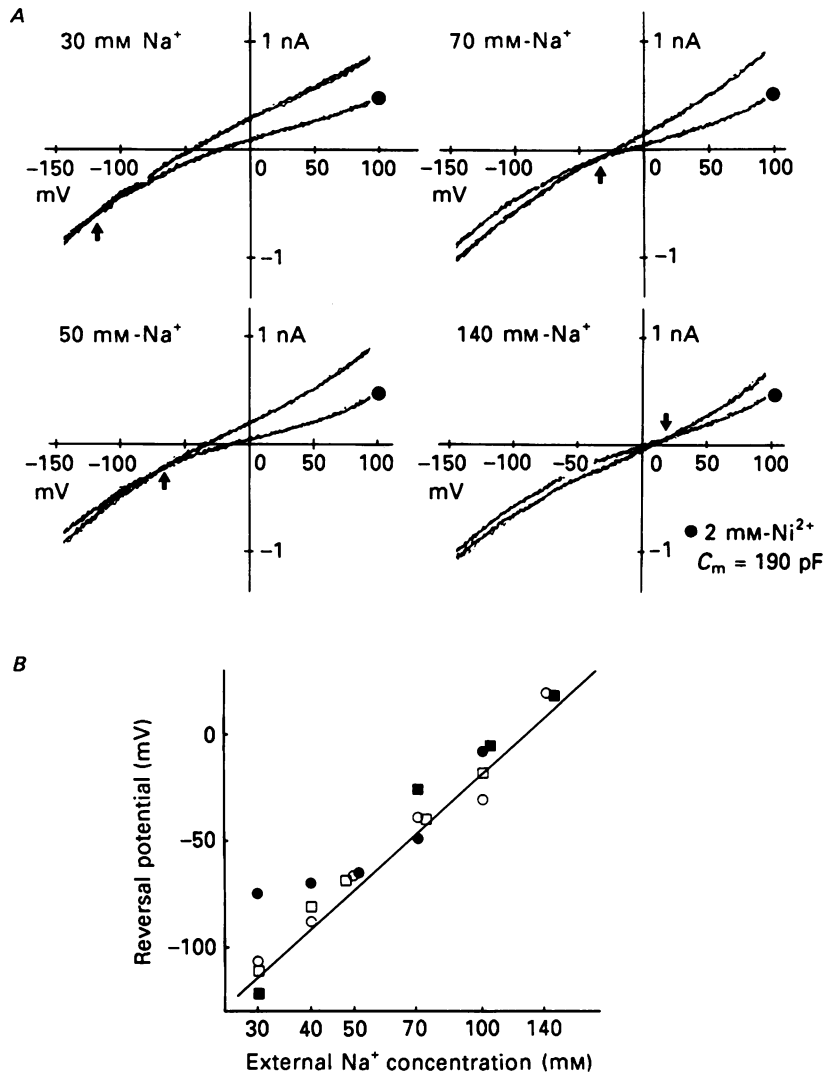

Fig. 12. *A*, *I–V* relations of Na^+-induced current obtained before and during (●) application of 2 mM-Ni^{2+}. *I–V* relations were determined at 30, 50, 70 and 140 mM $[Na^+]_o$ in the usual way and are plotted in a way similar to that in Fig. 7*B*. Other ionic conditions were 10 mM $[Na^+]_i$, 253 nM $[Ca^{2+}]_i$ and 0·5 mM $[Ca^{2+}]_o$. Arrows indicate intersection of the two families of *I–V* relations. *B*, reversal potential of Ni^{2+}-sensitive component of Na^+-induced current. Data from four cells are plotted against $[Na^+]_o$ on a semilogarithmic scale. Straight line shows theoretical equilibrium potential of Na^+–Ca^{2+} exchange given by stoichiometry of $3Na^+$:$1Ca^{2+}$. Different symbols indicate different cells.

DISCUSSION

In this investigation, the outward or inward current was induced by externally applying Ca^{2+} or Na^+ to internally perfused myocytes and the reversal potentials were measured at various concentrations of these ions. When the membrane potential was clamped at the equilibrium potential given by $3Na^+:1Ca^{2+}$ exchange, no significant change was observed in the holding current in response to the concentration changes. The Na^+–Ca^{2+} exchange current was isolated as the difference between the records obtained in the absence and presence of Ni^{2+}. The reversal potentials measured were in good agreement with the equilibrium potential predicted for $3Na^+:1Ca^{2+}$ exchange. Based on these results, we conclude that the Ca^{2+}- or Na^+-induced current is generated by the Na^+–Ca^{2+} exchange system, that the stoichiometry of the Na^+–Ca^{2+} exchange system is $3Na^+:1Ca^{2+}$, and that this ratio is constant in the range of $[Na^+]_o$ from 30 to 140 mM, $[Ca^{2+}]_o$ from 0·2 to 20 mM and $[Ca^{2+}]_i$ from 153 to 803 nM.

We found that the intracellular ionic conditions, at least in some limited subcellular spaces near the Na^+–Ca^{2+} exchanger, change relatively rapidly during activation of the Na^+–Ca^{2+} exchange. To avoid an error caused by this mechanism, in our measurements of the reversal potential, the holding potential was set at $E_{Na,Ca}$, as given from the ionic compositions of the pipette and bath solutions. Pipettes with a tip diameter of about 3–4 μm were used to facilitate equilibration of the internal solutions. We consider that the ionic concentrations in the intracellular space were practically equal to those in the pipette solution. Our conclusion that the stoichiometry is $3Na^+:1Ca^{2+}$ is in agreement with that of many workers.

The equilibrium potential and stoichiometry of Na^+–Ca^{2+} exchange system

The stoichiometry of the Na^+–Ca^{2+} exchange has been investigated using various methods. One approach was to measure the intracellular Na^+ and Ca^{2+} concentrations. Assuming that the Na^+ and Ca^{2+} fluxes are mainly through the Na^+–Ca^{2+} exchange, Blaustein & Hodgkin (1969) suggested that $3Na^+:1Ca^{2+}$ exchange was necessary to maintain $[Ca^{2+}]_i$ at less than 100 nM in resting squid axon. Mullins & Brinley (1975) suggested $4Na^+:1Ca^{2+}$ exchange using a similar method. Recently intracellular Na^+ and Ca^{2+} activities were measured using Na^+- and Ca^{2+}-sensitive microelectrodes in different tissues. The stoichiometry was reported to be 2·4–2·9 $Na^+:1Ca^{2+}$ in sheep heart Purkinje fibres (Bers & Ellis, 1982) and 2·5$Na^+:1Ca^{2+}$ in both sheep ventricular muscle and Purkinje strands (Sheu & Fozzard, 1982). Considering the role of the Na^+–K^+ pump at rest, the stoichiometry was suggested to be near $3Na^+:1Ca^{2+}$ exchange (Axelsen & Bridge, 1985; Sheu & Fozzard, 1985).

Measurement of ion flux in dialysed squid axon or barnacle single muscle fibre supported the $3Na^+:1Ca^{2+}$ exchange (Blaustein & Santiago, 1977; Rasgado-Flores & Blaustein, 1987). Similar results from flux measurements were reported in the rabbit ventricular myocardium (Bridge & Bassingthwaighte, 1983). Based on measurements of ion fluxes in cardiac membrane vesicle, many workers suggested the $3Na^+:1Ca^{2+}$ exchange (Pitts, 1979; Wakabayashi & Goshima, 1981; Reeves & Hale, 1984). Ledvora & Hegyvary (1983), however, concluded $4Na^+:1Ca^{2+}$ exchange from

determination of the reversal potential of the ion flux. Measurements of the Na^+–Ca^{2+} exchange current in the retinal rod outer segment by Yau & Nakatani (1984) and Hodgkin & Nunn (1987), or in the cardiac myocardium by Kimura *et al.* (1987), suggested a stoichiometry very close to $3Na^+$:$1Ca^{2+}$.

The above variation in the reported stoichiometry may suggest that the stoichiometry does change depending on experimental conditions, such as internal perfusion, isolated vesicles, different membrane potentials, internal and external ionic conditions etc. In our study, the reversal potentials obtained at different $[Ca^{2+}]_o$, $[Na^+]_o$ and $[Ca^{2+}]_i$ were well fitted with a line drawn on the basis of $3Na^+$: $1Ca^{2+}$ exchange, thereby suggesting that the stoichiometry is fixed at this ratio and is at least independent of these ion concentrations.

The agreement between the experimental and theoretical reversal potentials over a fairly wide range of potentials (−115 to +40 mV, Figs 8*B*, 11*B* and 12*B*) further suggests that the stoichiometry is also probably independent of the membrane potential. It could be speculated that the stoichiometry is determined by a deviation of the potential from $E_{Na,Ca}$. In this regard, however, the agreement of the stoichiometry obtained from the measurement of the reversal potential in our study with that based on the flux measurements (see above), which are performed at a membrane potential different from $E_{Na,Ca}$, may support the voltage-independent stoichiometry.

Changes in intracellular Ca^{2+} and Na^+ concentrations

The decay of the Na^+–Ca^{2+} exchange current in Figs 2 and 3 was attributed to Ca^{2+} accumulation and Na^+ depletion in the cell or around the carrier molecules. The following findings support this view. (1) When the capacity of the Ca^{2+} buffer in the internal solution was increased, the decay of the current became slower. (2) When the membrane potential was clamped at equilibrium potential during activation of the Na^+–Ca^{2+} exchange system, successive measurements of the *I–V* relations revealed little or no time-dependent change of the exchange current. (3) Kimura *et al.* (1987) reported that the Sr^{2+}-induced current decayed faster than the Ca^{2+}-induced one, which can be explained by the smaller stability constant of EGTA for Sr^{2+}.

Hume & Uehara (1986*a*, *b*) observed that in frog atrial cells an extra current was induced by intracellular Na^+ loading. This current also exhibited a time-dependent decay during depolarizing pulses, and its reversal potential shifted depending on amplitude and duration of the preceding depolarization. They suggested that this was the Na^+–Ca^{2+} exchange current, and attributed the time-dependent current decay to changes in ionic gradients across the membrane. The current decay in their experiment was much more rapid than that in our study, probably because Ca^{2+} buffer was absent in the internal solution.

Background current and divalent cations

The application of 10 mM $[Ca^{2+}]_o$ induced a slight outward shift of the holding current even at the holding potential of −85 mV, which was equal to $E_{Na,Ca}$ (Fig. 3). Kimura *et al.* (1986) reported a similar phenomenon that 1 mM $[Ca^{2+}]_o$ induced a slight outward shift in the holding current in the absence of internal Na^+ or in the

presence of external 0·1 mM-La^{3+}, which is known to block the Na^+–Ca^{2+} exchange. These phenomena are probably due to a decrease in background conductance, because external Ca^{2+} may inhibit the background current (Fig. 7). The depressing effect on the background conductance may be common among divalent cations, such as Ca^{2+}, Ba^{2+}, Mg^{2+} and probably Ni^{2+}. Another possible explanation for this phenomenon is that setting the holding potential at −85 mV in the presence of 0·1 mM $[Ca^{2+}]_o$ might change internal Na^+ and Ca^{2+} concentrations. The subsequent increase in $[Ca^{2+}]_o$ from 0·1 to 10 mM will result in generation of an outward current, because the equilibrium potential at 10 mM $[Ca^{2+}]_o$ at this moment is no longer −85 mV but should be more negative. This possibility, however, seems unlikely because the inward current was hardly generated at 0·1 mM $[Ca^{2+}]_o$ (Fig. 7).

Relation between the inward current and internal Ca^{2+} concentration

The Na^+–Ca^{2+} exchange system does not operate in the absence of internal Ca^{2+} (Baker & McNaughton, 1976; Allen & Baker, 1985; Kimura *et al.* 1987; DiPolo & Beaugé, 1987) and internal Ca^{2+} has a catalytic action on the Na^+–Ca^{2+} exchange system (Caroni & Carafoli, 1983). This mechanism, however, cannot explain our finding that the inward component of the Na^+–Ca^{2+} exchange current was sometimes small or not detectable when 153 nM $[Ca^{2+}]_i$ was used, because the outward current was consistently activated by increasing $[Ca^{2+}]_o$. Rather, the finding may be explained by assuming that the $[Ca^{2+}]_i$ of 153 nM was in some cells too low for the Ca^{2+} binding site of the exchanger to be occupied by internal Ca^{2+} and to generate a detectable amplitude of the inward Na^+–Ca^{2+} exchange current. This view may be supported by the findings that the inward component of Na^+–Ca^{2+} exchange current was consistently observed in 803 nM $[Ca^{2+}]_i$-loaded cells (Fig. 10) and that it had a tendency to increase with increases of $[Ca^{2+}]_i$, as may be noted by comparing Fig. 12 ($[Ca^{2+}]_i$ = 253 nM) with Fig. 10 ($[Ca^{2+}]_i$ = 803 nM).

Mechanism of Ni^{2+} action on Na^+–Ca^{2+} exchange system

The Lineweaver–Burk plot (Fig. 6) suggests that Ni^{2+} competes with Ca^{2+} for external Ca^{2+} binding sites of the carrier, and also binds at some different sites, thereby resulting in a depression of the carrier function. However, Ni^{2+} also inhibited the inward Na^+–Ca^{2+} exchange current. The following possibilities may explain the inhibition of the inward Na^+–Ca^{2+} exchange current by Ni^{2+}. (1) Ni^{2+} also acts on the Na^+ binding site. (2) Ni^{2+} inhibits the inward Na^+–Ca^{2+} exchange current in a non-competitive manner. (3) Ni^{2+} competes with Ca^{2+} for the Ca^{2+} binding site after the carrier has released Ca^{2+} from inside to outside the membrane. The mechanism has not been clarified.

The competitive action of Ni^{2+} with Ca^{2+} may reduce the probability that Ca^{2+} combines with the carrier. However, such a decrease in the 'effective' Ca^{2+} concentration does not necessarily change the reversal potential of the Na^+–Ca^{2+} exchange current, provided the carrier protein bound with Ni^{2+} cannot transport Ca^{2+} or Na^+. To clarify this point, we examined the effect of an inhibitor on the reversal potential of a Na^+–Ca^{2+} exchange model (Mullins, 1977). The reversal potential of the models remains unchanged in the presence of the inhibitor, whether its action is competitive or non-competitive. The agreement between the zero current

potential of the Ni^{2+}-sensitive current and the theoretical $E_{Na, Ca}$ in our experiments also supports the view that Ni^{2+} is neither transported by the carrier nor affects the reversal potential.

Voltage dependence of Na^+–Ca^{2+} exchange

The Ni^{2+}-sensitive current has a tendency to saturate at potentials negative to the reversal potential, but increases in amplitude exponentially or linearly with increases in depolarization beyond $E_{Na, Ca}$ at various $[Ca^{2+}]_o$ (Figs 8*A* and 11*A*). This tendency at potentials positive to the reversal potential probably reflects the intrinsic voltage dependence of the Na^+–Ca^{2+} exchange system itself, since no voltage-dependent action of Ni^{2+} was detected on the outward Na^+–Ca^{2+} exchange current. Such an exponential increase in the exchange current with membrane depolarizations is expected for a thermodynamic model of the Na^+–Ca^{2+} exchange proposed by Mullins (1977, 1981), but cannot be explained by the model proposed by Eisner & Lederer (1985).

The trend of saturation of the inward current with increasing hyperpolarizations is, however, reconciled with neither the thermodynamic model of Mullins nor the flux measurements which suggest large increases in Ca^{2+} fluxes with negative as well as positive deviations of the membrane potential from equilibrium potential (see Mullins, 1981). The finding might be related to a voltage-dependent change in the turnover rate of the exchanger (Eisner & Lederer, 1985), a depletion of Ca^{2+} within the cell during ramp pulses, a decrease of Ni^{2+} action on the inward current with membrane hyperpolarizations, or other unknown factors. Thus, we have no conclusion at present.

We thank Dr J. Kimura and Dr Y. Ikemoto for valuable discussions on this work. One of the authors (S.M.) is grateful to Professor H. Mashiba, Tottori University School of Medicine, for arranging the opportunity to work in the II Department of Physiology, Faculty of Medicine, Kyushu University. We also thank Mariko Ohara for comments on the manuscript and Fumiko Katsuda for secretarial services. This work was supported by research grants from the Ministry of Education, Science and Culture of Japan and from 'The Research Program on Cell Calcium Signals in the Cardiovascular System'.

REFERENCES

ALLEN, T. J. A. & BAKER, P. F. (1985). Intracellular Ca indicator Quin-2 inhibits Ca^{2+} inflow via Na_i/Ca_o exchange in squid axon. *Nature* **315**, 755–756.

AXELSEN, P. H. & BRIDGE, J. H. B. (1985). Electrochemical ion gradients and the Na/Ca exchange stoichiometry. Measurements of these gradients are thermodynamically consistent with a stoichiometric coefficient $\geqslant 3$. *Journal of General Physiology* **85**, 471–478.

BAHINSKI, A., NAKAO, M. & GADSBY, D. C. (1988). Potassium translocation by the Na/K pump is voltage insensitive. *Proceedings of the National Academy of Sciences of the USA* **85**, 3412–3416.

BAKER, P. F. & MCNAUGHTON, P. A. (1976). Kinetics and energetics of calcium efflux from intact squid giant axons. *Journal of Physiology* **259**, 103–144.

BERS, D. M. & ELLIS, D. (1982). Intracellular calcium and sodium activity in sheep heart Purkinje fibres. Effect of changes of external sodium and intracellular pH. *Pflügers Archiv* **393**, 171–178.

BLAUSTEIN, M. P. & HODGKIN, A. L. (1969). The effect of cyanide on the efflux of calcium from squid axons. *Journal of Physiology* **200**, 497–527.

BLAUSTEIN, M. P. & SANTIAGO, E. M. (1977). Effects of internal and external cations and of ATP on sodium–calcium and calcium–calcium exchange in squid axons. *Biophysical Journal* **20**, 79–111.

BRIDGE, J. H. B. & BASSINGTHWAIGHTE, J. B. (1983). Uphill sodium transport driven by an inward calcium gradient in heart muscle. *Science* **219**, 178–180.

CARONI, P. & CARAFOLI, E. (1983). The regulation of the Na^+–Ca^{2+} exchanger of heart sarcolemma. *European Journal of Biochemistry* **132**, 451–460.

DIPOLO, R. & BEAUGÉ, L. (1983). The calcium pump and sodium–calcium exchange in squid axons. *Annual Review of Physiology* **45**, 313–324.

DIPOLO, R. & BEAUGÉ, L. (1987). Characterization of the reverse Na/Ca exchange in squid axons and its modulation by Ca_i and ATP: Ca_i-dependent Na_i/Ca_o and Na_i/Na_o exchange modes. *Journal of General Physiology* **90**, 505–525.

EISNER, D. A. & LEDERER, W. J. (1985). Na–Ca exchange: stoichiometry and electrogenicity. *American Journal of Physiology* **248**, C189–202.

FABIATO, A. & FABIATO, F. (1979). Calculator programs for computing the composition of the solutions containing multiple metals and ligands used for experiments in skinned muscle cells. *Journal de physiologie* **75**, 463–505.

HAMILL, O. P., MARTY, A., NEHER, E., SAKMANN, B. & SIGWORTH, F. J. (1981). Improved patch-clamp techniques for high-resolution current recording from cells and cell-free membrane patches. *Pflügers Archiv* **391**, 85–100.

HODGKIN, A. L., MCNAUGHTON, P. A. & NUNN, B. J. (1987). Measurement of sodium–calcium exchange in salamander rods. *Journal of Physiology* **391**, 347–370.

HODGKIN, A. L. & NUNN, B. J. (1987). The effect of ions on sodium–calcium exchange in salamander rods. *Journal of Physiology* **391**, 371–398.

HUME, J. R. & UEHARA, A. (1986*a*). Properties of "creep currents" in single frog atrial cells. *Journal of General Physiology* **87**, 833–855.

HUME, J. R. & UEHARA, A. (1986*b*). "Creep currents" in single frog atrial cells may be generated by electrogenic Na/Ca exchange. *Journal of General Physiology* **87**, 857–884.

ISENBERG, G. & KLÖCKNER, U. (1982). Calcium tolerant ventricular myocytes prepared by preincubation in a "KB medium". *Pflügers Archiv* **395**, 6–18.

KIMURA, J., MIYAMAE, S. & NOMA, A. (1987). Identification of sodium–calcium exchange current in single ventricular cells of guinea-pig. *Journal of Physiology* **384**, 199–222.

KIMURA, J., NOMA, A. & IRISAWA, H. (1986). Na–Ca exchange current in mammalian heart cells. *Nature* **319**, 596–597.

LANGER, G. A. (1982). Sodium–calcium exchange in the heart. *Annual Review of Physiology* **44**, 435–449.

LEDVORA, R. F. & HEGYVARY, C. (1983). Dependence of Na^+–Ca^{2+} exchange and Ca^{2+}–Ca^{2+} exchange on monovalent cations. *Biochimica et biophysica acta* **729**, 123–136.

MULLINS, L. J. (1977). A mechanism for Na/Ca transport. *Journal of General Physiology* **70**, 681–695.

MULLINS, L. J. (1981). *Ion Transport in Heart*. New York: Raven Press.

MULLINS, L. J. & BRINLEY JR, F. J. (1975). Sensitivity of calcium efflux from squid axons to changes in membrane potential. *Journal of General Physiology* **65**, 135–152.

NAKAO, M. & GADSBY, D. C. (1986). Voltage dependence of Na translocation by the Na/K pump. *Nature* **323**, 628–630.

PHILIPSON, K. D. (1985). Sodium–calcium exchange in plasma membrane vesicles. *Annual Review of Physiology* **47**, 561–571.

PITTS, B. J. R. (1979). Stoichiometry of sodium–calcium exchange in cardiac sarcolemmal vesicles: coupling to the sodium pump. *Journal of Biological Chemistry* **254**, 6232–6235.

POWELL, T., TERRAR, D. A. & TWIST, V. W. (1980). Electrical properties of individual cells isolated from adult rat ventricular myocardium. *Journal of Physiology* **302** 131–153.

RASGADO-FLORES, H. & BLAUSTEIN, M. P. (1987). Na/Ca exchange in barnacle muscle cells has a stoichiometry of $3Na^+/1Ca^{2+}$. *American Journal of Physiology* **252**, C499–504.

REEVES, J. P. & HALE, C. C. (1984). The stoichiometry of the cardiac sodium–calcium exchange system. *Journal of Biological Chemistry* **259**, 7733–7739.

SATO, R., NOMA, A., KURACHI, Y. & IRISAWA, H. (1985). Effects of intracellular acidification on membrane currents in ventricular cells of the guinea pig. *Circulation Research* **57**, 553–561.

SHEU, S. & FOZZARD, H. A. (1982). Transmembrane Na^+ and Ca^{2+} electrochemical gradients in cardiac muscle and their relationship to force development. *Journal of General Physiology* **80**, 325–351.

SHEU, S. & FOZZARD, H. A. (1985). Na/Ca exchange in the intact cardiac cell. *Journal of General Physiology* **85**, 476–478.

SOEJIMA, M. & NOMA, A. (1984). Mode of regulation of the ACh-sensitive K-channel by the muscarinic receptor in rabbit atrial cells. *Pflügers Archiv* **400**, 424–431.

TANIGUCHI, J., KOKUBUN, S., NOMA, A. & IRISAWA, H. (1981). Spontaneously active cells isolated from the sino-atrial and atrio-ventricular nodes of the rabbit heart. *Japanese Journal of Physiology* **31**, 547–558.

TERADA, K. KITAMURA, K. & KURIYAMA, H. (1987). Blocking actions of Ca^{2+} antagonists on the Ca^{2+} channels in the smooth muscle cell membrane of rabbit small intestine. *Pflügers Archiv* **408**, 552–557.

TIBBITS, G. F. & PHILIPSON, K. D. (1985). Na^+-dependent alkaline earth metal uptake in cardiac sarcolemmal vesicles. *Biochimica et biophysica acta* **817**, 327–332.

TSIEN, R. Y. (1980). New calcium indicators and buffers with high selectivity against magnesium and protons: design, synthesis, and properties of prototype structures. *Biochemistry* **19**, 2396–2404.

TSIEN, R. Y. & RINK, T. J. (1980). Neutral carrier ion-selective microelectrodes for measurement of intracellular free calcium. *Biochimica et biophysica acta* **599**, 623–638.

WAKABAYASHI, S. & GOSHIMA, K. (1981). Kinetic studies on sodium-dependent calcium uptake by myocardial cells and neuroblastoma cells in culture. *Biochimica et biophysica acta* **642**, 158–172.

YAU, K. & NAKATANI, K. (1984). Electrogenic Na–Ca exchange in retinal rod outer segment. *Nature* **311**, 661–663.